Available at www.sciencedirect.com

INFORMATION PROCESSING IN AGRICULTURE 4 (2017) 128–139

journal homepage: www.elsevier.com/locate/inpa

Analyzing drying characteristics and modeling of thin layers of peppermint leaves under hot-air and infrared treatments

Seyed-Hassan Miraei Ashtiani[*], *Alireza Salarikia*, *Mahmood Reza Golzarian*

Department of Biosystems Engineering, Faculty of Agriculture, Ferdowsi University of Mashhad, Mashhad, Iran

ARTICLE INFO

Article history:
Received 21 January 2017
Received in revised form
28 February 2017
Accepted 2 March 2017
Available online 9 March 2017

Keywords:
Drying kinetics
Effective diffusivity
Energy activation
Moisture ratio
Moisture removal
Semi-theoretical model

ABSTRACT

The drying kinetics of peppermint leaves was studied to determine the best drying method for them. Two drying methods include hot-air and infrared techniques, were employed. Three different temperatures (30, 40, 50 °C) and air velocities (0.5, 1, 1.5 m/s) were selected for the hot-air drying process. Three levels of infrared intensity (1500, 3000, 4500 W/m^2), emitter-sample distance (10, 15, 20 cm) and air speed (0.5, 1, 1.5 m/s) were used for the infrared drying technique. According to the results, drying had a falling rate over time. Drying kinetics of peppermint leaves was explained and compared using three mathematical models. To determine coefficients of these models, non-linear regression analysis was used. The models were evaluated in terms of reduced chi-square (χ^2), root mean square error (RMSE) and coefficient of determination (R^2) values of experimental and predicted moisture ratios. Statistical analyses indicated that the model with the best fitness in explaining the drying behavior of peppermint samples was the Logarithmic model for hot-air drying and Midilli model for infrared drying. Moisture transfer in peppermint leaves was also described using Fick's diffusion model. The lowest effective moisture diffusivity (1.096×10^{-11} m^2/s) occurred during hot-air drying at 30 °C using 0.5 m/s, whereas its highest value (5.928×10^{-11} m^2/s) belonged to infrared drying using 4500 W/m^2 infrared intensity, 0.5 m/s airflow velocity and 10 cm emitter-sample distance. The activation energy for infrared and hot-air drying were ranged from 0.206 to 0.439 W/g, and from 21.476 to 27.784 kJ/mol, respectively.

1. Introduction

Medicinal herbs are globally prepared and used by human beings. Peppermint (*Mentha piperita* L.) is an important, widely-used aromatic medicinal plant [1]. As a medicinal plant, peppermint leaves should be dried in order to be ready for storage and consumption [2]. The drying process helps reaching two goals: first its inhibits the growth of microorganisms, and, second, it facilitates the storage and transportation of these plants [3,4]. Drying accounts for the highest energy-consumption in the food industry [5]. This is due to the high latent heat required for water vaporization and also the thermo-physical properties of the drying materials [6]. Therefore, developing an efficient drying method is essential for

* Corresponding author at: Department of Biosystems Engineering, Faculty of Agriculture, Ferdowsi University of Mashhad, P.O. Box 9177948978, Mashhad, Iran.
E-mail address: Miraei_sh@yahoo.com (S.-H. Miraei Ashtiani).
Peer review under responsibility of China Agricultural University.
http://dx.doi.org/10.1016/j.inpa.2017.03.001

energy utilization and conservation [3]. Plants can be dehydrated by a variety of methods. The hot-air drying technique is a widely-applied drying technique thanks to its simple implementation, low requirements for investment and operating costs [7]. This technique, however, have high thermal energy requirements with a long drying time, which changes the dried product in an undesirable manner [8–10]. Accordingly, the last decade was marked with several efforts in researching and developing alternative drying techniques for agricultural products [8,11].

The infrared technology is practically an alternative method. It is mainly adopted due to its adaptability, equipment simplicity, fast heating and drying, inexpensive and uncomplicated installation and use. Infrared drying is widely-applied as an alternative technique for drying fresh agricultural products [12]. In infrared drying, the electromagnetic energy collided with and infiltrated into the samples, where it turned into heat [5,7,13,14]. The moisture reduction process in the hot-air drying technique is as follows: The ambient heat migrates to the food surface through convection, and penetrates through the inside of food by conduction. Thus water migrates from the inner parts of the food to the interface between air and food through diffusion. It also reaches the air stream from the interface through convection [15]. Infrared radiation heating has more advantages than the hot-air technique such as better energy efficiency, and higher rates of heat transfer and flux. Thus the former has a shorter drying time and a faster drying rate [7]. It is suitable specifically for samples with thin layers, which have a large surface area exposed to radiation [12]. Moreover, infrared drying consumes up to 50% less energy than convective drying [16].

To integrate experimental knowledge from research on food drying into industrial applications, drying kinetics should be modeled mathematically. A mathematical model can be also used to optimize the management of parameters in practice and to predict the performance of a drying system [17]. Drying involves complex thermal processes in which mass and heat are transferred simultaneously, in a coupled manner and unsteadily both inside and on the surface of a sample. Accordingly, one should have a thorough understanding of the control parameters in this process [18,19]. In the literature, the drying behavior is described through three mathematical models: theoretical, semi-theoretical and empirical [3,17,18,20]. An understanding of the underlying phenomena and mechanisms of the drying process helps develop different theoretical models [21]. In Liu et al. [8], Karim and Hawlader [22], and Goula et al. [23], both theoretical models and computational simulations were applied to as a means to predict drying curves of different products. They stated that theoretical results were in good agreement with experimental outputs. Theoretical simulations are realistic and are able to explain the phenomena that occur in the process. On the other hand, these simulations are hard to carry out and require a great computing time. This is because diffusion equations governing the process are very complicated [24]. Empirical models can be developed from the direct correlation of moisture content (MC) with the drying time, without taking principles of this process into account [3]. Accordingly, empirically-developed models can predict drying curves for real-world settings. Their parameters, however, do not have any physical bearing and fail to accurately explain the important process phenomena [25]. As a trade-off between theory and convenient application, semi-theoretical models are extracted from simplified Fick's second law of diffusion or they are derived by modifying any simplified widely-used model [26].

The literature review showed few studies on drying kinetics and mathematical modeling of peppermint [2,21]. The aim of this work was to examine the drying behavior of peppermint leaves by hot-air and infrared drying methods and to find the best drying model that explains the hot-air and infrared drying of peppermint leaves. Also, the effective moisture diffusivities and activation energies of both processes in drying peppermint leaves were determined.

2. Materials and methods

2.1. Material preparation

Fresh peppermint leaves were harvested freshly before each series of experiments from the research field of Ferdowsi University of Mashhad, Iran. Leaves were selected based on visual assessment of their uniform color and size. Leaves were always picked in the morning after morning dew has dried. Peppermint leaves were kept in cooled bags before reaching the laboratory. Initial MC of samples was determined by drying three 30 g samples of fresh leaves in an electric convection oven at 105 °C for a total period of 24 h [27]. Their initial MC was 82.17 ± 0.2% (w.b.). The thick stems of samples were precisely cut before experiments.

2.2. Drying equipment

For this study, a prototype dryer was developed in the department of biosystems engineering, Ferdowsi University, Mashhad, Iran. Fig. 1 schematically shows the study dryer. It consisted of a drying chamber, control units for air flow, temperature and infrared radiation, an electric heater, air inlet and outlet ducts, an air filter, and an electrical fan. The drying chamber was made of sheet aluminum with a $0.5^{L} \times 0.5^{W} \times 0.4^{H}$ m^3 cavity and a front door for handling the sample tray. Its outer surface was completely insulated to prevent ambient heat losses. The incoming air was preheated using an electric 2000-W heater at the inlet duct. The heater power-control unit was used to adjust air temperature. The temperature inside the drying chamber was continuously monitored by a thermocouple (type K, ±1 °C) which was embedded in the control component. Air was directed through a series of electrical resistance heaters to reach higher temperatures and was then redirected towards the drying chamber. The drying air flows horizontally over the samples in this configuration. A blower creating axial flow and a module for controlling its rotation speed were used to adjust air velocity. A digital hot wire anemometer (TESTO 425, ±0.03 m/s, made in Germany) was used to measure the air velocity. There were three 250-W infrared lamps (Philips, made in China) mounted on the upper side of the drying chamber. The height of lamps was adjustable using height adjustment screws. Their infrared radiation intensity was regulated using an autotransformer. A solarimeter (Casella 187010b-02, made in the UK) was

Fig. 1 – Experimental setup. (1 – fresh air inlet, 2 – air filter, 3 – heater, 4 – adjustment screws, 5 – infrared lamps, 6 – sample tray, 7 – digital balance, 8 – fan, 9 – air outlet, 10 – desktop computer, 11 – control unit).

employed to measure the infrared radiation intensity. A digital scale (AND, GF 6000, made in Japan) with a repeatability of ±0.01 g was put under the drying tray and was linked to a computer and its related software in order to capture and record weight outputs at fixed 1 min intervals.

2.3. *Drying experiments*

Different airflow velocities at three levels of 0.5, 1 and 1.5 m/s and temperatures at three levels of 30, 40 and 50 °C were selected for hot-air drying experiments. Moreover, different levels of radiation intensity (1500, 3000 and 4500 W/m^2), emitter-sample distance (10, 15 and 20 cm) and airflow velocity (0.5, 1 and 1.5 m/s) were employed for infrared drying. The air temperature and airflow velocity values were selected based on the available research literature on industrial air drying applications, particularly on the drying of leafy vegetables and medicinal plants in thin-layers [14,28]. As a rule of thumb, low temperatures should be used for drying these products (*i.e.* 30–50 °C) in order to obtain an optimized product quality [20]. Prior to each experiment, the dryer was left idle for a period of about 30 min to provide a steady state based on predetermined experimental drying conditions [8]. For each treatment, 200 ± 1 g of the leaves were spread uniformly in a thin-layer on a perforated aluminum tray (40 × 40 cm). Drying was terminated once sample MCs reached the target 10% (w.b.). All the drying treatments were conducted in three replications. Drying curves were then drawn using mean moisture ratios at each time point.

2.4. *Mathematical modeling*

The drying data of peppermint leaves were fitted into three semi-theoretical thin-layer drying models (see Table 1), which are widely employed for determining the drying curves. The dimensionless moisture ratio (MR) of peppermint leaves was given by Eq. (1) [29]:

$$MR = \frac{M_t - M_e}{M_0 - M_e} \quad (1)$$

where M_t, M_0 and M_e are MC at any given time, initial MC and equilibrium MC (% w.b.), respectively.

For longer drying times, M_e is fairly smaller than M_0 and M_t, and Eq. (1) can be simplified to Eq. (2) [12,20,30]:

$$MR = M_t/M_0 \quad (2)$$

Data were analyzed in SPSS 22 (IBM SPSS Statistics, IBM Corporation, Armonk, NY, USA) using non-linear regression analysis and thus the model coefficients were determined. The goodness of fit of the models was determined through statistical parameters, *e.g.* the reduced chi-square (χ^2), coefficient of determination (R^2), and root mean square error (RMSE) between experimental and model data. The model's goodness of fit can be indicated by having high coefficients of determination and low values for χ^2 and RMSE [19]. The R^2 value was determined using Eq. (3) [3], and χ^2 and RMSE parameters were computed using Eqs. (4) and (5), respectively [19]:

$$R^2 = \frac{\sum_{i=1}^{N}(MR_i - MR_{pre,i}) \cdot \sum_{i=1}^{N}(MR_i - MR_{exp,i})}{\sqrt{\left[\sum_{i=1}^{N}(MR_i - MR_{pre,i})^2\right] \cdot \left[\sum_{i=1}^{N}(MR_i - MR_{exp,i})^2\right]}} \quad (3)$$

$$\chi^2 = \frac{\sum_{i=1}^{N}(MR_{exp,i} - MR_{pre,i})^2}{N - z} \quad (4)$$

$$RMSE = \left[\frac{1}{N}\sum_{i=1}^{N}(MR_{exp,i} - MR_{pre,i})^2\right]^{\frac{1}{2}} \quad (5)$$

where MR_{exp} and MR_{pre} are dimensionless moisture ratios, respectively, obtained from experiment and modeling, N is

Table 1 – Mathematical models used to express the temporal variation of moisture content in thin layer drying process.

Model number	Model name	Model equation	References
1	Lewis	$MR = \exp(-kt)$	Shi et al. [19]
2	Logarithmic	$MR = a\exp(-kt) + c$	Balasubramanian et al. [35]
3	Midilli	$MR = a\exp(-kt^n) + bt$	Arslan et al. [2]

the number of observations, z is the number of constants in a model and i is the number of terms.

2.5. Determination of effective moisture diffusivity

As a key transport feature when modeling the drying process for various agricultural materials, the effective moisture diffusivity is a function of drying temperature and product MC [18]. For samples having slab geometry, Fick's diffusion equation was applied to determine this parameter using the method of slopes [31]. The peppermint samples were considered having a slab geometry due to their flat surface and less than or equal to 0.25 mm thickness. The equation was as follows [19]:

$$MR = \frac{8}{\pi^2}\sum_{n=0}^{\infty}\frac{1}{(2n+1)^2}\times\exp\left[\frac{-(2n+1)^2\pi^2 D_{eff}t}{4L^2}\right] \quad (6)$$

where D_{eff} stands for the effective diffusivity coefficient (m^2/s), L is half of the thickness of the sample (m), n can be a positive integer, and t shows the duration of the drying process (s).

In case of longer drying times, Eq. (6) can be shortened to Eq. (7) which includes only the first term of the series. This would have no considerable effect on prediction accuracy [12].

$$\ln(MR) = \ln\left(\frac{8}{\pi^2}\right) - \left(\frac{\pi^2 D_{eff}t}{4L^2}\right) \quad (7)$$

The effective moisture diffusivity can be extracted from a diagram showing the drying data from the experiments as ln (MR) against time. From Eq. (7), the ln(MR)-time diagram would present an inclined line with its slope (K) given by the following equation [2]:

$$K = \frac{\pi^2 D_{eff}}{4L^2} \quad (8)$$

The effective moisture diffusivity is also determined using this equation.

2.6. Computation of activation energy

Bonding potential of moisture in non-dry materials is a main player in determining, their drying characteristics. The bonding potential of moisture is quantified by the value of activation energy, which is the energy required for eliminating 1 mol moisture from the substance with constant compositions and given MC [32]. The activation energy of the hot-air technique is obtained from the simple Arrhenius equation, as follows [9,18]:

$$D_{eff} = D_0\exp\left(-\frac{E_a}{R(T+273.15)}\right) \quad (9)$$

where T is the drying air temperature (°C), R is the universal gas constant (8.314×10^{-3} kJ mol^{-1} K^{-1}), D_0 is the pre-exponential factor of the Arrhenius equation (m^2/s), and E_a is the activation energy (kJ/mol).

Eq. (9) can be rearranged into the form of Eq. (10):

$$\ln(D_{eff}) = \ln(D_0) - \frac{E_a}{R(T+273.15)} \quad (10)$$

E_a is derived from the slope of a straight line when $\ln(D_{eff})$ is plotted against the multiplicative inverse of absolute temperature ($1/(T+273.15)$). A modified form of the Arrhenius equation was used as it is impossible to accurately measure infrared drying temperature (Eq. (11)) [12]:

$$D_{eff} = D_0\exp\left(-\frac{E_a m}{P}\right) \quad (11)$$

where m is the sample weight (g), E_a is the activation energy (W/g), and P is the infrared output power (W).

3. Results and discussion

3.1. Drying curves

The time requirements for drying peppermint leaves under different conditions of this study were given in details in our previous work [33]. Graphs of experimental data from drying peppermint leaves using the hot-air technique with different temperatures (30, 40 and 50 °C) and airflow velocities (0.5, 1 and 1.5 m/s) were analyzed in terms of reduction in moisture ratio (MR) with drying time (Fig. 2). This is because MR curves are better in explaining the drying behavior of products than MC curves [3], as the starting MR for all experiments was set at one. The shape of hot-air drying curves for peppermints is similar to that for other hot-air-dried food materials. This shows moisture removal of samples is faster during the early stages of the drying process, which decreases as the drying time increases. MR continued to decrease over the drying time. From falling MR values it can be concluded that diffusion can probably control the internal moisture transfer [34]. That is, no constant-rate drying interval was observed in the exponential curves as all the drying experiments followed a falling rate. This suggests that internal diffusion was the dominant process for controlling mass transfer [19]. Results were in accordance with the findings reported by Doymaz [18], Khazaei et al. [20] and Ben Haj Said et al. [31] for hot-air drying of persimmon slices, avishan leaves and rosy garlic leaves, respectively. As typical of all thermally activated processes, the slope of the drying curve increased at higher temperatures and, consequently, the required drying time before reaching the target MC decreased. In fact, water molecules moved faster at higher heat transfer rates caused by an increased drying temperature. This, in turn, accelerated moisture movement inside samples [19]. Similar results were reported in the literature on other bio-products [4,35]. ANOVA

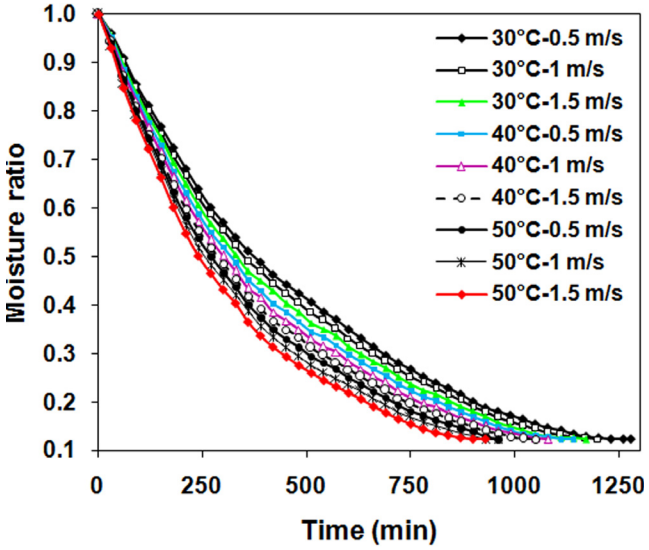

Fig. 2 – Moisture ratio variations as a function of time for hot-air drying of peppermint leaves.

results showed that the temperature had the most significant effect on drying kinetics ($p < 0.05$) of samples. Airflow velocity had the second most significant effect. As shown in Fig. 2, drying curves became steeper with increasing airflow velocity. Higher air velocities led to faster drying by improving convective heat and mass transfer coefficients between the sample and its ambient air [36]. These findings are supported by other authors [19,20]. Effects of ambient temperature and airflow velocity on the drying kinetics became negligible at the later stages of drying when water movement inside sample became difficult, and mass transfer became a limiting factor. There are numerous factors hindering the mass transfer process including solute concentration, crust formation and product hardening [4].

Infrared drying curves of peppermint leaves dried under different settings are given in Fig. 3. During drying, the moisture removal rate decreases and triggers the falling-rate period. There was no period with constant moisture removal rate under all experimental conditions. This is mainly due to the fact that the sample had no constant supply of water during the whole process [30]. The MR reduction followed an exponential trend during drying for all scenarios (Fig. 3). The effect of infrared radiation level on MR of samples was significant ($p < 0.5$) as predicted (Fig. 3). At both constant airflow velocity and emitter-sample distance, MR decreased faster when infrared radiation level raised. This result is in agreement with those reported in the literature [30,37]. This is because higher infrared radiation levels have higher infrared energy, which consequently increases temperature and vapor pressure of the sample MC and eventually, its moisture removal rate [30]. Airflow velocity also was effective in drying characteristics of peppermint leaves. The infrared drying results showed that, unlike hot-air drying, MR decreased faster with reducing the airflow velocity, at similar infrared radiation intensity and emitter-sample distance. Results of Sharma et al. [14] support these results. Increases airflow

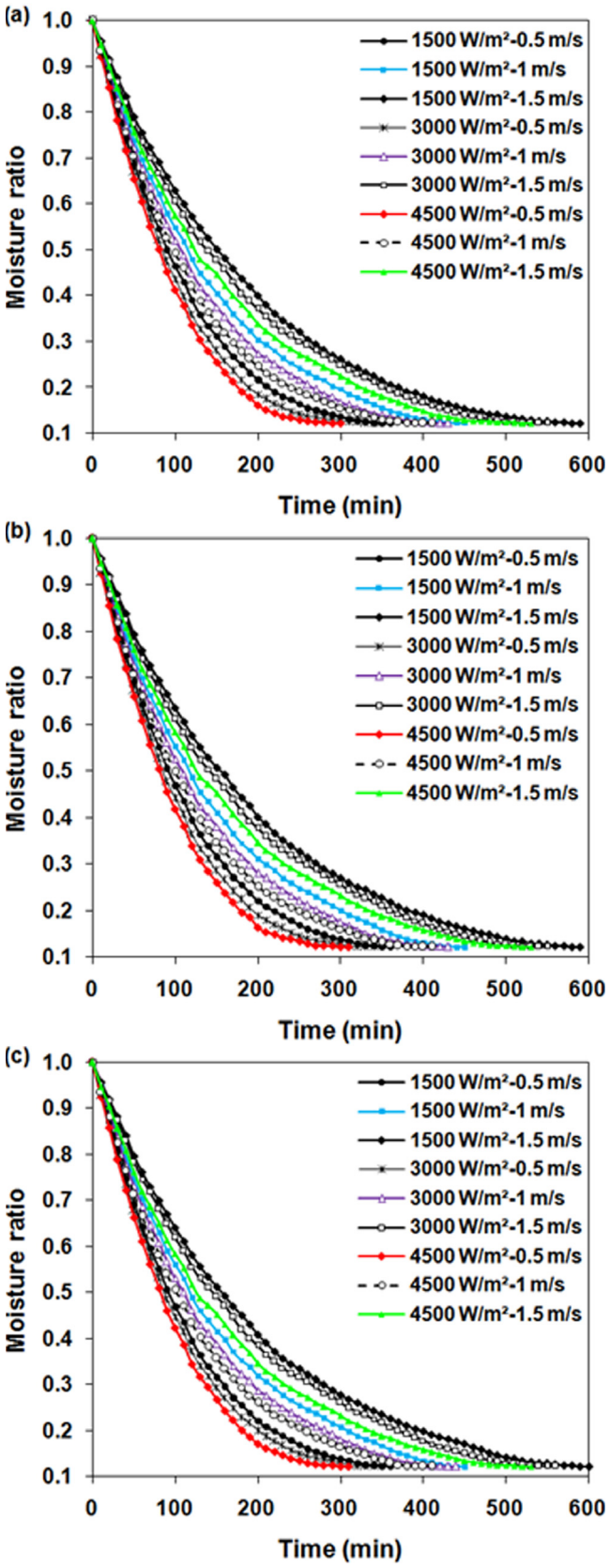

Fig. 3 – The moisture ratio-time relationship during infrared drying at different infrared intensities, air velocities and (a) 10 cm, (b) 15 cm and (c) 20 cm emitter-sample distances.

velocity accelerated the cooling effect that reduced the product temperature. Less mass transfer was a result of reduction in vapor pressure or driving force of the moisture [37]. At similar infrared radiation intensity and airflow velocity, MR reduction becomes faster when the infrared emitter is placed closer to the sample. As the sample-radiator distance increases, the heat radiation hits the sample surface but does not penetrate effectively into the inside of the leaves. Therefore, the absorbed energy of the moisture inside the sample leaves decreases dramatically [8]. Accordingly, moisture removal rate decreased by increasing the distance between infrared emitter and sample. That is, the distance had a significant effect on moisture evaporation from the samples. The results displayed that the radiation distance had a larger effect on drying kinetics of peppermint leaves than airflow velocity. In sum, it is fair to conclude that infrared drying of peppermint leaves using a smaller emitter-sample distance, higher infrared radiation intensity and lower airflow velocity enhances moisture removal leading to effective dehydration.

3.2. *Mathematical modeling of drying curves*

As discussed earlier, the MC results from all experiments were converted to the MR, and after that curves were fitted into drying time of three drying models from the literature (Table 1). Table 2 lists the results obtained from analyzing these models for hot-air drying. Table 2 presents all the models with acceptable R2 (more than 0.98) under all drying conditions, whereas the highest R^2 values belonged to the Logarithmic model. At the same time, the lowest RMSE and chi-square values also belonged to this model. Hence, amongst the applied models, the Logarithmic model was

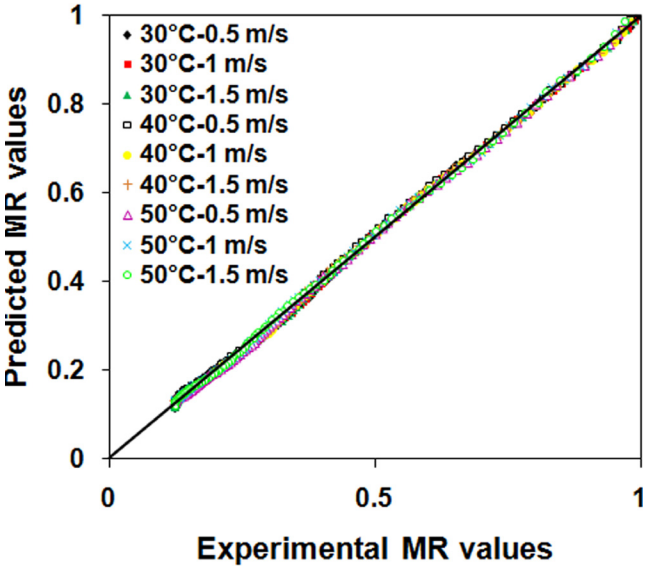

Fig. 4 – Experimental vs. predicted moisture ratios using the Logarithmic model for hot-air drying at various air velocities and temperatures.

Table 2 – Results of statistical analysis on the models for moisture contents as a function of drying time for the hot-air dried peppermint leaves.

Models	Drying conditions	Estimated parameters	$\chi^2 \times 10^{-4}$	RMSE	R^2
1	T: 30 °C, V: 0.5 m/s	k: 0.001782	0.63	0.00792	0.99952
	T: 30 °C, V: 1 m/s	k: 0.001869	0.88	0.00934	0.99939
	T: 30 °C, V: 1.5 m/s	k: 0.001958	1.34	0.01154	0.99917
	T: 40 °C, V: 0.5 m/s	k: 0.002053	1.88	0.01366	0.99894
	T: 40 °C, V: 1 m/s	k: 0.002154	2.33	0.01520	0.99875
	T: 40 °C, V: 1.5 m/s	k: 0.002266	2.84	0.01677	0.98055
	T: 50 °C, V: 0.5 m/s	k: 0.002393	2.73	0.01645	0.99855
	T: 50 °C, V: 1 m/s	k: 0.002515	2.97	0.01716	0.99843
	T: 50 °C, V: 1.5 m/s	k: 0.002657	3.18	0.01773	0.98834
2	T: 30 °C, V: 0.5 m/s	k: 0.001908, a: 0.982284, c: 0.027212	0.36	0.00591	0.99972
	T: 30 °C, V: 1 m/s	k: 0.002032, a: 0.972937, c: 0.034808	0.38	0.00610	0.99970
	T: 30 °C, V: 1.5 m/s	k: 0.002182, a: 0.962574, c: 0.045071	0.43	0.00641	0.99967
	T: 40 °C, V: 0.5 m/s	k: 0.002345, a: 0.953045, c: 0.054919	0.40	0.00625	0.99968
	T: 40 °C, V: 1 m/s	k: 0.002504, a: 0.946676, c: 0.061666	0.40	0.00621	0.99968
	T: 40 °C, V: 1.5 m/s	k: 0.002676, a: 0.941495, c: 0.067329	0.35	0.00584	0.99972
	T: 50 °C, V: 0.5 m/s	k: 0.002830, a: 0.941007, c: 0.068535	0.36	0.00595	0.99970
	T: 50 °C, V: 1 m/s	k: 0.002995, a: 0.942177, c: 0.069391	0.32	0.00556	0.99974
	T: 50 °C, V: 1.5 m/s	k: 0.003174, a: 0.942772, c: 0.069404	0.30	0.00541	0.99976
3	T: 30 °C, V: 0.5 m/s	k: 0.002361, a: 1.018975, b: 0.000005, n: 0.960821	0.39	0.00619	0.99969
	T: 30 °C, V: 1 m/s	k: 0.002741, a: 1.021206, b: 0.000005, n: 0.944774	0.45	0.00661	0.99965
	T: 30 °C, V: 1.5 m/s	k: 0.002924, a: 1.021099, b: 0.000012, n: 0.943921	0.48	0.00682	0.99962
	T: 40 °C, V: 0.5 m/s	k: 0.003073, a: 1.020568, b: 0.000021, n: 0.945489	0.43	0.00650	0.99965
	T: 40 °C, V: 1 m/s	k: 0.003194, a: 1.019747, b: 0.000028, n: 0.948325	0.40	0.00628	0.99967
	T: 40 °C, V: 1.5 m/s	k: 0.003267, a: 1.018219, b: 0.000037, n: 0.954366	0.36	0.00598	0.99970
	T: 50 °C, V: 0.5 m/s	k: 0.003268, a: 1.016231, b: 0.000043, n: 0.963207	0.41	0.00627	0.99967
	T: 50 °C, V: 1 m/s	k: 0.003128, a: 1.013532, b: 0.000052, n: 0.980204	0.37	0.00599	0.99970
	T: 50 °C, V: 1.5 m/s	k: 0.003115, a: 1.011156, b: 0.000058, n: 0.990815	0.35	0.00577	0.99973

T, V, χ^2, RMSE and R^2 are air temperature, air velocity, reduced chi-square, root mean square error and coefficient of determination, respectively.

Table 3 – Results of statistical analysis on the models for moisture contents as a function of drying time for the infrared dried peppermint leaves.

Models	Drying conditions	Estimated parameters	$\chi^2 \times 10^{-4}$	RMSE	R^2
1	IR: 1500 W/m^2, V: 0.5 m/s, D: 10 cm	k: 0.007405	4.41	0.02072	0.99744
	IR: 1500 W/m^2, V: 0.5 m/s, D: 15 cm	k: 0.007292	4.10	0.01996	0.99763
	IR: 1500 W/m^2, V: 0.5 m/s, D: 20 cm	k: 0.007122	4.35	0.02058	0.99756
	IR: 1500 W/m^2, V: 1 m/s, D: 10 cm	k: 0.005689	3.88	0.01948	0.98819
	IR: 1500 W/m^2, V: 1 m/s, D: 15 cm	k: 0.005600	3.54	0.01861	0.99836
	IR: 1500 W/m^2, V: 1 m/s, D: 20 cm	k: 0.005496	3.48	0.01846	0.99841
	IR: 1500 W/m^2, V: 1.5 m/s, D: 10 cm	k: 0.004398	3.55	0.01869	0.99833
	IR: 1500 W/m^2, V: 1.5 m/s, D: 15 cm	k: 0.004307	3.42	0.01833	0.99847
	IR: 1500 W/m^2, V: 1.5 m/s, D: 20 cm	k: 0.004217	3.65	0.01894	0.97841
	IR: 3000 W/m^2, V: 0.5 m/s, D: 10 cm	k: 0.008050	5.28	0.02265	0.99674
	IR: 3000 W/m^2, V: 0.5 m/s, D: 15 cm	k: 0.007940	4.67	0.02131	0.99712
	IR: 3000 W/m^2, V: 0.5 m/s, D: 20 cm	k: 0.007792	4.17	0.02012	0.97744
	IR: 3000 W/m^2, V: 1 m/s, D: 10 cm	k: 0.006192	4.81	0.02168	0.99767
	IR: 3000 W/m^2, V: 1 m/s, D: 15 cm	k: 0.006098	4.45	0.02086	0.99785
	IR: 3000 W/m^2, V: 1 m/s, D: 20 cm	k: 0.005972	4.60	0.02120	0.99780
	IR: 3000 W/m^2, V: 1.5 m/s, D: 10 cm	k: 0.004702	3.96	0.01972	0.99836
	IR: 3000 W/m^2, V: 1.5 m/s, D: 15 cm	k: 0.004615	3.63	0.01887	0.99848
	IR: 3000 W/m^2, V: 1.5 m/s, D: 20 cm	k: 0.004519	3.54	0.01864	0.99849
	IR: 4500 W/m^2, V: 0.5 m/s, D: 10 cm	k: 0.008708	3.44	0.01824	0.99772
	IR: 4500 W/m^2, V: 0.5 m/s, D: 15 cm	k: 0.008559	3.93	0.01951	0.99743
	IR: 4500 W/m^2, V: 0.5 m/s, D: 20 cm	k: 0.008435	3.43	0.01823	0.99774
	IR: 4500 W/m^2, V: 1 m/s, D: 10 cm	k: 0.006710	6.51	0.02521	0.95666
	IR: 4500 W/m^2, V: 1 m/s, D: 15 cm	k: 0.006598	5.96	0.02412	0.99701
	IR: 4500 W/m^2, V: 1 m/s, D: 20 cm	k: 0.006463	5.36	0.02287	0.99734
	IR: 4500 W/m^2, V: 1.5 m/s, D: 10 cm	k: 0.005101	5.65	0.02355	0.99761
	IR: 4500 W/m^2, V: 1.5 m/s, D: 15 cm	k: 0.004985	5.57	0.02338	0.96772
	IR: 4500 W/m^2, V: 1.5 m/s, D: 20 cm	k: 0.004863	5.43	0.02309	0.99780
2	IR: 1500 W/m^2, V: 0.5 m/s, D: 10 cm	k: 0.008948, a: 0.953805, c: 0.067667	0.88	0.00901	0.99938
	IR: 1500 W/m^2, V: 0.5 m/s, D: 15 cm	k: 0.008790, a: 0.953048, c: 0.067575	0.75	0.00829	0.99948
	IR: 1500 W/m^2, V: 0.5 m/s, D: 20 cm	k: 0.008644, a: 0.950038, c: 0.070136	0.65	0.00772	0.99954
	IR: 1500 W/m^2, V: 1 m/s, D: 10 cm	k: 0.006848, a: 0.938365, c: 0.071762	0.17	0.00399	0.99987
	IR: 1500 W/m^2, V: 1 m/s, D: 15 cm	k: 0.006693, a: 0.938707, c: 0.070128	0.18	0.00407	0.98987
	IR: 1500 W/m^2, V: 1 m/s, D: 20 cm	k: 0.006567, a: 0.936673, c: 0.071098	0.19	0.00421	0.99986
	IR: 1500 W/m^2, V: 1.5 m/s, D: 10 cm	k: 0.005242, a: 0.942251, c: 0.067798	0.18	0.00419	0.99986
	IR: 1500 W/m^2, V: 1.5 m/s, D: 15 cm	k: 0.005126, a: 0.939167, c: 0.068723	0.11	0.00322	0.99992
	IR: 1500 W/m^2, V: 1.5 m/s, D: 20 cm	k: 0.005041, a: 0.935969, c: 0.070885	0.11	0.00330	0.98991
	IR: 3000 W/m^2, V: 0.5 m/s, D: 10 cm	k: 0.009714, a: 0.961651, c: 0.064736	1.82	0.01291	0.99876
	IR: 3000 W/m^2, V: 0.5 m/s, D: 15 cm	k: 0.009526, a: 0.961336, c: 0.063544	1.51	0.01176	0.99897
	IR: 3000 W/m^2, V: 0.5 m/s, D: 20 cm	k: 0.009321, a: 0.960434, c: 0.063350	1.21	0.01054	0.99917
	IR: 3000 W/m^2, V: 1 m/s, D: 10 cm	k: 0.007567, a: 0.939287, c: 0.074503	0.28	0.00511	0.99979
	IR: 3000 W/m^2, V: 1 m/s, D: 15 cm	k: 0.007418, a: 0.939239, c: 0.073709	0.24	0.00472	0.99982
	IR: 3000 W/m^2, V: 1 m/s, D: 20 cm	k: 0.007283, a: 0.938040, c: 0.074640	0.23	0.00462	0.99983
	IR: 3000 W/m^2, V: 1.5 m/s, D: 10 cm	k: 0.005606, a: 0.934554, c: 0.070046	0.17	0.00399	0.99987
	IR: 3000 W/m^2, V: 1.5 m/s, D: 15 cm	k: 0.005483, a: 0.935450, c: 0.069245	0.16	0.00384	0.99988
	IR: 3000 W/m^2, V: 1.5 m/s, D: 20 cm	k: 0.005365, a: 0.936495, c: 0.068891	0.17	0.00407	0.99987
	IR: 4500 W/m^2, V: 0.5 m/s, D: 10 cm	k: 0.009932, a: 0.980582, c: 0.044741	2.14	0.01392	0.99862
	IR: 4500 W/m^2, V: 0.5 m/s, D: 15 cm	k: 0.009951, a: 0.974771, c: 0.051562	2.07	0.01369	0.97865
	IR: 4500 W/m^2, V: 0.5 m/s, D: 20 cm	k: 0.009742, a: 0.975297, c: 0.049787	1.68	0.01274	0.99883
	IR: 4500 W/m^2, V: 1 m/s, D: 10 cm	k: 0.008421, a: 0.939049, c: 0.080582	0.55	0.00714	0.99960
	IR: 4500 W/m^2, V: 1 m/s, D: 15 cm	k: 0.008228, a: 0.937678, c: 0.079778	0.42	0.00622	0.99969
	IR: 4500 W/m^2, V: 1 m/s, D: 20 cm	k: 0.008002, a: 0.937150, c: 0.078600	0.33	0.00553	0.99976
	IR: 4500 W/m^2, V: 1.5 m/s, D: 10 cm	k: 0.006261, a: 0.929643, c: 0.077781	0.20	0.00439	0.99984
	IR: 4500 W/m^2, V: 1.5 m/s, D: 15 cm	k: 0.006127, a: 0.926091, c: 0.079703	0.13	0.00353	0.99990
	IR: 4500 W/m^2, V: 1.5 m/s, D: 20 cm	k: 0.005971, a: 0.923569, c: 0.080789	0.18	0.00409	0.99986

Table 3 – (*continued*)

Models	Drying conditions	Estimated parameters	$\chi^2 \times 10^{-4}$	RMSE	R^2
3	*IR*: 1500 W/m^2, *V*: 0.5 m/s, *D*: 10 cm	*k*: 0.005171, *a*: 0.994660, *b*: 0.000239, *n*: 1.100865	0.06	0.00234	0.99996
	IR: 1500 W/m^2, *V*: 0.5 m/s, *D*: 15 cm	*k*: 0.005281, *a*: 0.995883, *b*: 0.000233, *n*: 1.092799	0.06	0.00226	0.99996
	IR: 1500 W/m^2, *V*: 0.5 m/s, *D*: 20 cm	*k*: 0.005427, *a*: 0.997352, *b*: 0.000226, *n*: 1.082351	0.07	0.00255	0.99995
	IR: 1500 W/m^2, *V*: 1 m/s, *D*: 10 cm	*k*: 0.006044, *a*: 1.004100, *b*: 0.000142, *n*: 1.010095	0.15	0.00371	0.99989
	IR: 1500 W/m^2, *V*: 1 m/s, *D*: 15 cm	*k*: 0.006276, *a*: 1.005902, *b*: 0.000129, *n*: 0.998369	0.18	0.00407	0.99987
	IR: 1500 W/m^2, *V*: 1 m/s, *D*: 20 cm	*k*: 0.006460, *a*: 1.007265, *b*: 0.000122, *n*: 0.988614	0.19	0.00415	0.99986
	IR: 1500 W/m^2, *V*: 1.5 m/s, *D*: 10 cm	*k*: 0.004182, *a*: 0.999057, *b*: 0.000113, *n*: 1.029654	0.04	0.00196	0.99997
	IR: 1500 W/m^2, *V*: 1.5 m/s, *D*: 15 cm	*k*: 0.004569, *a*: 1.002442, *b*: 0.000103, *n*: 1.008464	0.08	0.00267	0.99994
	IR: 1500 W/m^2, *V*: 1.5 m/s, *D*: 20 cm	*k*: 0.004898, *a*: 1.005630, *b*: 0.000095, *n*: 0.991534	0.12	0.00329	0.99991
	IR: 3000 W/m^2, *V*: 0.5 m/s, *D*: 10 cm	*k*: 0.004522, *a*: 0.989216, *b*: 0.000277, *n*: 1.148830	0.19	0.00415	0.99987
	IR: 3000 W/m^2, *V*: 0.5 m/s, *D*: 15 cm	*k*: 0.004706, *a*: 0.990746, *b*: 0.000267, *n*: 1.136529	0.14	0.00358	0.99991
	IR: 3000 W/m^2, *V*: 0.5 m/s, *D*: 20 cm	*k*: 0.004896, *a*: 0.992807, *b*: 0.000258, *n*: 1.123641	0.09	0.00288	0.99994
	IR: 3000 W/m^2, *V*: 1 m/s, *D*: 10 cm	*k*: 0.005849, *a*: 1.000817, *b*: 0.000175, *n*: 1.036234	0.10	0.00299	0.99993
	IR: 3000 W/m^2, *V*: 1 m/s, *D*: 15 cm	*k*: 0.005954, *a*: 1.002005, *b*: 0.000168, *n*: 1.028877	0.12	0.00326	0.99992
	IR: 3000 W/m^2, *V*: 1 m/s, *D*: 20 cm	*k*: 0.006050, *a*: 1.003374, *b*: 0.000161, *n*: 1.021525	0.15	0.00372	0.99989
	IR: 3000 W/m^2, *V*: 1.5 m/s, *D*: 10 cm	*k*: 0.005550, *a*: 1.004393, *b*: 0.000102, *n*: 0.987866	0.17	0.00394	0.99987
	IR: 3000 W/m^2, *V*: 1.5 m/s, *D*: 15 cm	*k*: 0.005601, *a*: 1.006071, *b*: 0.000096, *n*: 0.982072	0.16	0.00384	0.99988
	IR: 3000 W/m^2, *V*: 1.5 m/s, *D*: 20 cm	*k*: 0.005440, *a*: 1.006356, *b*: 0.000094, *n*: 0.983654	0.18	0.00406	0.99987
	IR: 4500 W/m^2, *V*: 0.5 m/s, *D*: 10 cm	*k*: 0.004378, *a*: 0.987373, *b*: 0.000277, *n*: 1.169912	0.39	0.00585	0.99976
	IR: 4500 W/m^2, *V*: 0.5 m/s, *D*: 15 cm	*k*: 0.004425, *a*: 0.988239, *b*: 0.000281, *n*: 1.165152	0.31	0.00519	0.99981
	IR: 4500 W/m^2, *V*: 0.5 m/s, *D*: 20 cm	*k*: 0.004531, *a*: 0.989318, *b*: 0.000271, *n*: 1.155899	0.25	0.00468	0.99984
	IR: 4500 W/m^2, *V*: 1 m/s, *D*: 10 cm	*k*: 0.005661, *a*: 0.999120, *b*: 0.000218, *n*: 1.063486	0.10	0.00299	0.99993
	IR: 4500 W/m^2, *V*: 1 m/s, *D*: 15 cm	*k*: 0.005939, *a*: 1.000729, *b*: 0.000206, *n*: 1.049218	0.13	0.00342	0.99991
	IR: 4500 W/m^2, *V*: 1 m/s, *D*: 20 cm	*k*: 0.006093, *a*: 1.001957, *b*: 0.000194, *n*: 1.038684	0.15	0.00366	0.99989
	IR: 4500 W/m^2, *V*: 1.5 m/s, *D*: 10 cm	*k*: 0.005903, *a*: 1.004416, *b*: 0.000127, *n*: 0.995053	0.18	0.00403	0.99987
	IR: 4500 W/m^2, *V*: 1.5 m/s, *D*: 15 cm	*k*: 0.006194, *a*: 1.006460, *b*: 0.000121, *n*: 0.981139	0.13	0.00353	0.99990
	IR: 4500 W/m^2, *V*: 1.5 m/s, *D*: 20 cm	*k*: 0.006430, *a*: 1.008330, *b*: 0.000113, *n*: 0.968744	0.16	0.00390	0.99987

IR, *V*, *D*, χ^2, RMSE and R^2 are infrared radiation intensity, air velocity, distance between emitter and sample, reduced chi-square, root mean square error and coefficient of determination, respectively.

selected as the model that has best results in predicting the drying behavior of peppermint leaves. Accordingly, values of R^2, χ^2 and RMSE of the Logarithmic model varied between 0.99967 to 0.99976, 0.000030 to 0.000043 and 0.00541 to 0.00641, respectively. The accuracy of the hot-air drying model was examined by comparing the predicted and experimental MR values. Fig. 4 compares experimental MR values with the values from the Logarithmic model for the peppermint leaves dried by different drying strategies. According to this figure, most of the predicted data were focused around a straight line. This shows the suitability of the Logarithmic model for explaining the kinetics of drying peppermint leaves using the hot-air drying method. This is in agreement with the previously published research results showing the capability of the Logarithmic model in explaining the drying behavior of different natural materials, for example jujube slices [16], betel leaves [35] and banana slices [38].

In infrared drying process, these three mathematical models, shown in Table 1, were also fitted into the drying data. Estimation results for different parameters as well as statistical data are given in Table 3. The R^2 values for the models under all conditions were greater than 0.96. This shows the capability of the models in explaining the behavior of peppermint leaves in infrared drying. Statistical analysis results indicated that R^2, χ^2 and RMSE variations were between 0.95666 and 0.99997, 0.000004 and 0.000651, and 0.00196 and 0.02521, respectively. Midilli model had best results in terms of R^2 (highest) and χ^2 and RMSE (lowest) between all thin-layer drying models. Therefore, the Midilli model was found to explain best the infrared drying of peppermint leaves. As shown, R^2, χ^2 and RMSE for this model ranged between 0.99976 and 0.99997, 0.000004 and 0.000039, and 0.00196 and 0.00585, respectively. The model was validated using charts indicating experimental and the model predicted moisture ratios as shown in Fig. 5. MR values both from experiments and model predictions had a very good agreement. As shown in the figure, data are mainly placed around a 45°-straight line. This shows that Midilli model is the best model for describing the infrared drying kinetics of peppermint leaves. Midilli model has been used by other researchers to explain infrared drying of sea cucumber [9] and peach slices [12].

3.3. *Effective moisture diffusivity*

The effective moisture diffusivity (D_{eff}) of foods represents their intrinsic moisture mass transfer characteristics consisting of different parameters like liquid diffusion, molecular diffusion, hydrodynamic flow, vapor diffusion and other mass transport mechanisms [10,13]. Fig. 6 presents D_{eff} values calculated from Eq. (8) under different temperatures and airflow velocities. D_{eff} for hot-air-dried peppermint leaves was between 1.096×10^{-11} and 2.486×10^{-11} m^2/s. This range is consistent with other hot-air-dried products particularly leafy material (*e.g.* 0.196×10^{-11} to 1.362×10^{-11} m^2/s for avishan leaves [20] and 0.91×10^{-11} to 10.41×10^{-11} m^2/s for mint leaves [39]). According to Torki-Harchegani et al. [21], D_{eff} of hot-air-dried peppermint leaves (at 50–70 °C) ranges from 1.809×10^{-9} to 4.649×10^{-9} m^2/s. They showed that D_{eff}

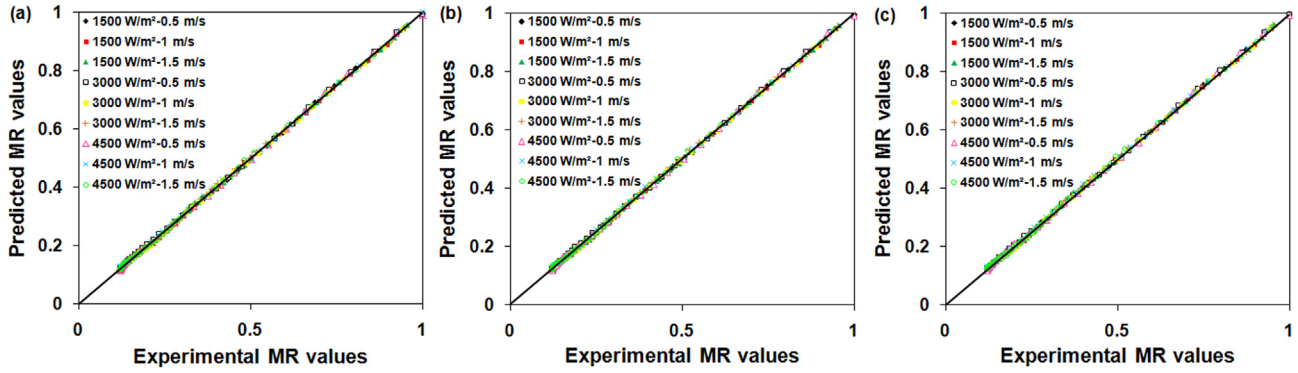

Fig. 5 – Experimental vs. predicted moisture ratios using Midilli model for infrared drying at different infrared intensities, air velocities and (a) 10 cm, (b) 15 cm and (c) 20 cm emitter-sample distances.

values for microwave-dried peppermint leaves were from 39.555×10^{-9} to 110.552×10^{-9} m^2/s. In a study by Arslan et al. [2], D_{eff} values for peppermint leaves under both solar and oven drying processes were 3.10×10^{-12} m^2/s and 2.68×10^{-12} m^2/s, respectively. These differences can be caused by the different properties of biomaterials (*e.g.* variety, composition and dimensions), different dryer conditions, drying techniques, physical or chemical pretreatment, initial MCs, and D_{eff} computation model [19,31]. Expectedly, values of D_{eff} increased as the drying temperature rose. This was due to the increase in vapor pressure of samples that accelerated moisture transfer at higher temperatures. By drying peppermint leaves at a higher temperature, the heating energy increases leading to increased activity among water molecules. As a result, higher D_{eff} values can be obtained [19]. Using higher airflow velocities at all drying temperatures leads to higher D_{eff} values. This might be due to lower vapor pressure as a result of higher airflow velocity, which in turn reduces the resistance to evaporation. These are in agreement with the literature findings that reported D_{eff} increases with increasing the drying temperature and airflow velocity [31]. The lowest D_{eff} occurred when using an airflow velocity of 0.5 m/s at 30 °C; whereas its largest value was reported when using 50 °C drying air flowing at 1.5 m/s. These results showed that higher air temperatures and velocities are preferred for drying peppermint leaves when using hot-air drying under given experimental settings. This is mainly due to the fact that D_{eff} values are relatively higher. The air temperature effect on D_{eff} of peppermint leaves was more than that airflow velocity. Using multiple regression, D_{eff} values were correlated to air temperature (T) and airflow velocity (V) through the following model:

$$D_{eff} = 10^{-12} \times (0.1127T + 6.197V + 0.0052T^2 - 1.3V^2 + 0.2633), \quad R^2 = 0.9977 \tag{12}$$

The calculated D_{eff} values for peppermint leaves under infrared drying process are shown in Fig. 7. As shown, these values range between 3.312×10^{-11} and 5.928×10^{-11} m^2/s. It can be seen from Fig. 7 that, D_{eff} increased when infrared intensity increased at a constant airflow velocity and a constant distance between emitter and sample. This can be caused by increased infrared radiation intensity levels that rapidly raised sample temperature. As a result, vapor pressure also increased, bringing about faster drying [12]. Research on button mushroom slices [5] also showed the similar effects of infrared intensity on D_{eff}. As shown in Fig. 7, D_{eff} was enhanced at lower emitter-sample distances under constant airflow velocity and infrared radiation intensity. Findings suggested that increasing airflow velocity under constant infrared radiation intensity and emitter-sample distance would lessen D_{eff}. This is due to the fact that faster airflow cools down the sample surface while sample's inside temperature remained relatively higher than the surface and surrounding air. This results in negative temperature gradient [13]. Airflow velocity has been reported to have a similar effect on D_{eff} during infrared drying of longans [37]. For infrared drying, the lowest D_{eff} was recorded at airflow velocity of 1.5 m/s, radiation intensity of 1500 W/m^2 and distance between emitter and sample of 20 cm, whereas the largest D_{eff} was recorded at 0.5 m/s airflow velocity, 4500 W/m^2 illumination intensity and a gap of 10 cm between the emitter and samples. Using multiple regression, D_{eff} values were correlated to airflow velocity (V), infrared radiation intensity (IR) and emitter-sample distance (D) through the following model:

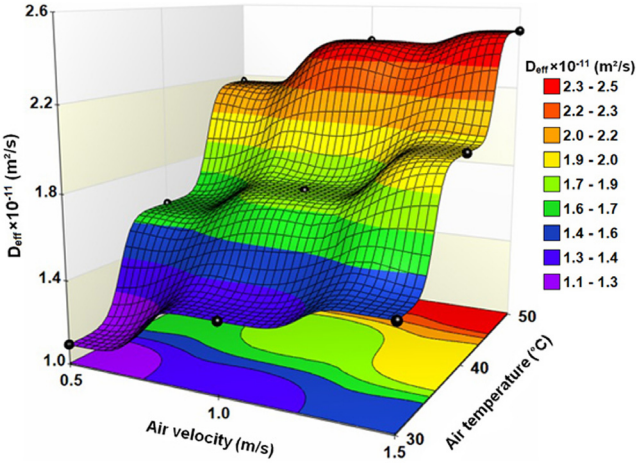

Fig. 6 – Interaction between air velocity and temperature on the effective diffusivity in hot-air drying of peppermint leaves.

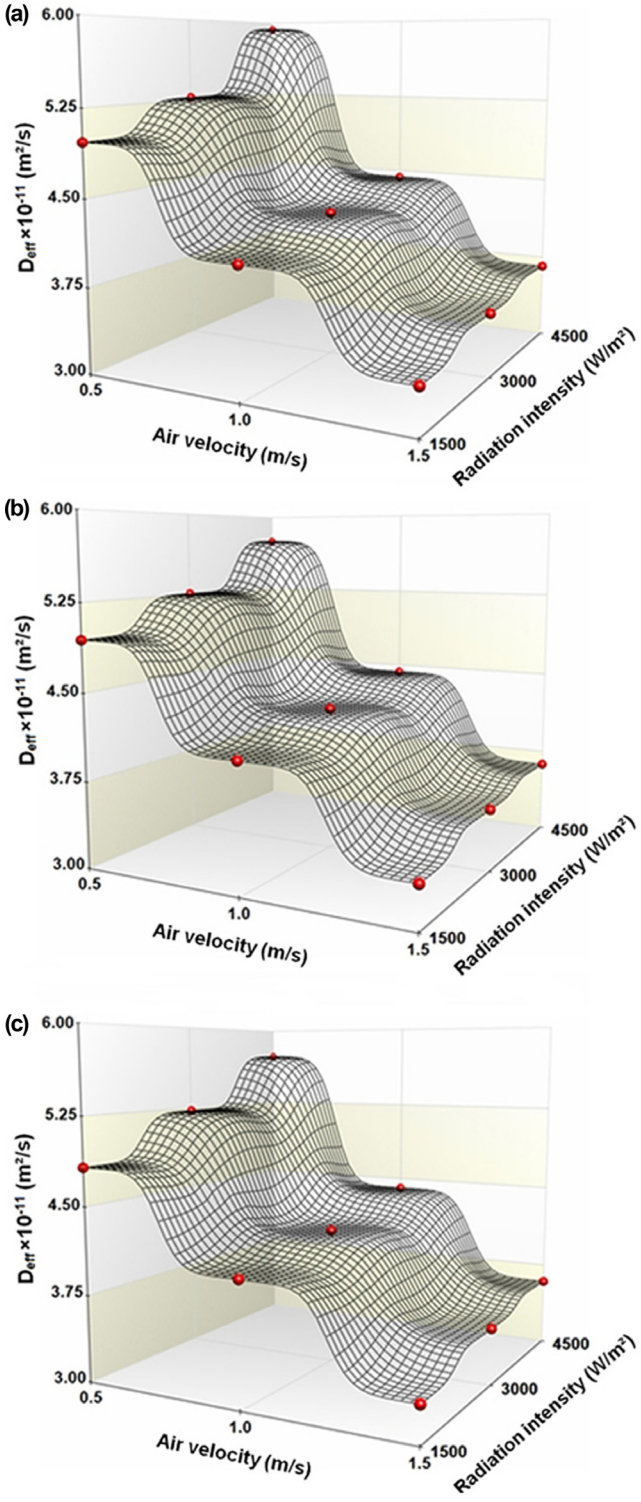

Fig. 7 – Variations of effective diffusivity from the effects of infrared radiation intensity, air velocity and (a) 10 cm, (b) 15 cm and (c) 20 cm emitter-sample distances.

$$D_{eff} = 10^{-10} \times (0.6177 + (1.14 \times 10^{-5} IR \times V) + (-0.2162V) + (-1.248 \times 10^{-7}) \times \exp(-6.875D)), \quad R^2 = 0.9665 \qquad (13)$$

The D_{eff} values from this research were within the overall range of 10^{-12} to 10^{-8} m²/s for drying biological materials [18]. D_{eff} was reduced as the drying time was extended. Accordingly, the largest D_{eff} values belonged to infrared drying experiments. This is mainly because drying is completed in much shorter time in an infrared dryer than in a hot-air drying system. Therefore, the infrared drying method performed more efficiently in drying peppermint leaves than hot-air drying. This finding is in agreement with the results obtained from previous research on sea cucumber [9] and jujube slices [16].

3.4. Activation energy

In hot-air drying, the activation energy was found to be 27.784, 24.122 and 21.476 kJ/mol for drying air velocity of 0.5, 1 and 1.5 m/s, respectively. These values are lower than the activation energies of 38.6–51.1 kJ/mol for avishan leaves [20], 46.80–52.68 kJ/mol for rosy garlic leaves [31], 79.873–109.003 kJ/mol for nettle leaves [36] and 32.65 kJ/mol for banana slices [38]. On the other hand, the values of activation energy were found to be greater than those of 13.48–16.50 kJ/mol for sweet potatoes slices [26] and 12.50 kJ/mol for drumstick leaves [40]; and around the same values as those of 30.64 kJ/mol for persimmon slices [18], 30.00 kJ/mol for yacon slices [19] and 22.01–30.99 kJ/mol for green peas [41]. In general, the activation energy, when drying food and agricultural products, ranges between 12.7–110 kJ/mol [42].

The computation results showed that in the infrared drying, the values of activation energy for peppermint leaves varied from 0.206 to 0.439 W/g for different air velocities and emitter-sample distances (Fig. 8). It is clearly seen that, unlike in the hot-air drying, activation energy values generally decreased with increasing air velocity in the infrared drying. In Fig. 8, the values of activation energy were plotted versus air velocities and distances between emitter and sample. The multiple regression analysis was used and the equation of fitted model and corresponding R^2 were found to be as follows:

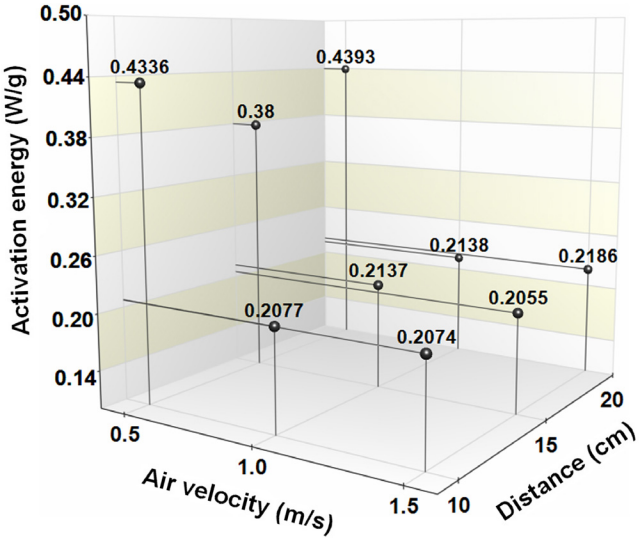

Fig. 8 – The influence of air velocity and distance between emitter and sample on energy activation value for infrared drying of peppermint leaves.

$$E_a = -3.594 + (15.769V) + (-17.912V^2) + (6.107V^3) + (-0.024D) + (0.001D^2), \quad R^2 = 0.9697 \tag{14}$$

In our research, it was found that the activation energy for infrared drying was noticeably lower as opposed to hot-air drying. This indicates that the energy requirement for samples dried by infrared drying is significantly less than those dried by hot-air drying.

4. Conclusions

The drying kinetics of peppermint leaves in two drying methods of hot-air and infrared were analyzed and modeled. In both drying methods, moisture removal was observed during the lessening-rate period and not during the constant-rate period. This implies that internal diffusion controls the moisture removal from the samples. The efficiency of infrared drying was better than that of hot-air drying thanks to the higher drying rate of the former. The drying data was fitted into different models, namely; Lewis, Logarithmic and Midilli. Statistical analyses showed that the Logarithmic and Midilli models, which had higher R^2 values and lower χ^2 and RMSE values, were the best models for predicting the drying characteristics of hot-air- and infrared-dried peppermint leaves, respectively. To gain a deeper insight about the mass transfer mechanism of peppermint leaves during drying process, the effective moisture diffusivity (D_{eff}) was also determined. It was found that the D_{eff} values ranged from 1.096×10^{-11} to 2.486×10^{-11} m^2/s and 3.312×10^{-11} to 5.928×10^{-11} m^2/s for hot-air and infrared drying, respectively. In hot-air drying, the value of D_{eff} was obtained to be larger at hotter temperatures and higher airflow velocities. In infrared drying, however, increasing infrared intensity and decreasing airflow velocity and emitter-sample distance led to higher D_{eff} values. The energy required to activate the moisture transfer from the inside of the leaves throughout the infrared and hot-air drying processes were in the range of 0.206 to 0.439 W/g and 21.476 to 27.784 kJ/mol, respectively. This study contributed to the literature by presenting useful insights on industrial drying of peppermint leaves. Before commercialization, further research is required to analyze the drying kinetics in the combined system of hot air and infrared drying within the experimental range of this research.

REFERENCES

[1] Uribe E, Marín D, Vega-Gálvez A, Quispe-Fuentes I, Rodríguez A. Assessment of vacuum-dried peppermint (*Mentha piperita* L.) as a source of natural antioxidant. Food Chem 2016;190:559–65.

[2] Arslan D, Özcan MM, Menges HO. Evaluation of drying methods with respect to drying parameters, some nutritional and color characteristics of peppermint (*Mentha* x *piperita* L.). Energy Convers Manage 2010;51(12):2769–75.

[3] Taghian Dinani S, Hamdami N, Shahedi M, Havet M. Mathematical modeling of hot air/electrohydrodynamic (EHD) drying kinetics of mushroom slices. Energy Convers Manage 2014;86:70–80.

[4] Chkir I, Balti MA, Ayed L, Azzouz S, Kechaou N, Hamdi M. Effects of air drying properties on drying kinetics and stability of cactus/brewer's grains mixture fermented with lactic acid bacteria. Food Bioprod Process 2015;94:10–9.

[5] Doymaz İ. Infrared drying of button mushroom slices. Food Sci Biotechnol 2014;23(3):723–9.

[6] Hii CL, Law CL, Law MC. Simulation of heat and mass transfer of cocoa beans under stepwise drying conditions in a heat pump dryer. Appl Therm Eng 2013;54(1):264–71.

[7] Liu Y, Miao S, Wu J, Liu J, Yu H, Duan X. Drying characteristics and modeling of vacuum far-infrared radiation drying of *Flos Lonicerae*. J Food Process Preserv 2015;39(4):338–48.

[8] Liu Y, Zhu W, Luo L, Li X, Yu H. A mathematical model for vacuum far-infrared drying of potato slices. Dry Technol 2014;32(2):180–9.

[9] Moon JH, Kim MJ, Chung DH, Pan CH, Yoon WB. Drying characteristics of sea cucumber (*Stichopus japonicas Selenka*) using far infrared radiation drying and hot air drying. J Food Process Preserv 2014;38(4):1534–46.

[10] Nachaisin M, Jamradloedluk J, Niamnuy C. Application of combined far-infrared radiation and air convection for drying of instant germinated brown rice. J Food Process Eng 2016;39 (3):306–18.

[11] Martynenko A, Zheng W. Electrohydrodynamic drying of apple slices: energy and quality aspects. J Food Eng 2016;168:215–22.

[12] Doymaz I. Suitability of thin-layer drying models for infrared drying of peach slices. J Food Process Preserv 2014;38 (6):2232–9.

[13] Pathare PB, Sharma GP. Effective moisture diffusivity of onion slices undergoing infrared convective drying. Biosyst Eng 2006;93(3):285–91.

[14] Sharma GP, Verma RC, Pathare P. Mathematical modeling of infrared radiation thin layer drying of onion slices. J Food Eng 2005;71(3):282–6.

[15] Demiray E, Tulek Y. The effect of pretreatments on air drying characteristics of persimmons. Heat Mass Transfer 2017;53 (1):99–106.

[16] Chen Q, Bi J, Wu X, Yi J, Zhou L, Zhou Y. Drying kinetics and quality attributes of jujube (*Zizyphus jujuba* Miller) slices dried by hot-air and short- and medium-wave infrared radiation. LWT-Food Sci Technol 2015;64(2):759–66.

[17] Puente-díaz L, Ah-Hen K, Vega-Gálvez A, Lemus-Mondaca R, Di Scala K. Combined infrared-convective drying of murta (*Ugni molinae* Turcz) berries: kinetic modeling and quality assessment. Dry Technol 2013;31(3):329–38.

[18] Doymaz İ. Evaluation of some thin-layer drying models of persimmon slices (*Diospyros kaki* L.). Energy Convers Manage 2012;56:199–205.

[19] Shi Q, Zheng Y, Zhao Y. Mathematical modeling on thin-layer pump drying of yacon (Smallanthus sonchifolius) slices. Energy Convers Manage 2013;71:208–16.

[20] Khazaei J, Arabhosseini A, Khosrobeygi Z. Application of superposition technique for modeling drying behavior of avishan (Zataria Multiflora) leaves. Trans ASABE 2008;51 (4):1383–93.

[21] Torki-Harchegani M, Ghanbarian D, Ghasemi Pirbalouti A, Sadeghi M. Dehydration behaviour, mathematical modelling, energy efficiency and essential oil yield of peppermint leaves undergoing microwave and hot air treatments. Renew Sustain Energy Rev 2016;58:407–18.

[22] Karim MA, Hawlader MNA. Drying characteristics of banana: theoretical modeling and experimental validation. J Food Eng 2005;70(1):35–45.

[23] Goula AM, Chasekioglou AN, Lazarides HN. Drying and shrinkage kinetics of solid waste of olive oil processing. Dry Technol 2015;33(14):1728–38.

[24] Sarsavadia PN, Sawhney RL, Pangavhane DR, Singh SP. Drying behaviour of brined onion slices. J Food Eng 1999;40(3):219–26.
[25] Simal S, Femenia A, Garau MC, Rosselló C. Use of exponential, Page's and diffusional models to simulate the drying kinetics of kiwi fruit. J Food Eng 2005;66(3):323–8.
[26] Fan K, Chen L, He J, Yan F. Characterization of thin layer hot air drying of sweet potatoes (*Ipomoea batatas* L.) slices. J Food Process Preserv 2015;39(6):1361–71.
[27] Tarhan S, Telci I, Tuncay MT, Polatci H. Product quality and energy consumption when drying peppermint by rotary drum dryer. Ind Crops Prod 2010;32(3):420–7.
[28] Buchaillot A, Caffin N, Bhandari B. Drying of lemon myrtle (*Backhousia citriodora*) leaves: retention of volatiles and color. Dry Technol 2009;27(3):445–50.
[29] Ng MX, Tham TC, Ong SP, Law CL. Drying kinetics of technical specified rubber. Inf Process Agric 2015;2(1):64–71.
[30] Supmoon N, Noomhorm A. Influence of combined hot air impingement and infrared drying on drying kinetics and physical properties of potato chips. Dry Technol 2013;31 (1):24–31.
[31] Ben Haj Said L, Najjaa H, Farhat A, Neffati M, Bellagha S. Thin layer convective air drying of wild edible plant (*Allium roseum*) leaves: experimental kinetics, modeling and quality. J Food Sci Technol 2015;52(6):3739–49.
[32] Fang S, Wang Z, Hu X. Hot air drying of whole fruit Chinese jujube (*Zizyphus jujube* Miller): thin-layer mathematical modelling. Int J Food Sci Technol 2009;44(9):1818–24.
[33] Salarikia A, Miraei Ashtiani SH, Golzarian MR. Comparison of drying characteristics and quality of peppermint leaves using different drying methods. J Food Process Preserv 2016. http://dx.doi.org/10.1111/jfpp.12930.
[34] Borah A, Hazarika K, Khayer SM. Drying kinetics of whole and sliced turmeric rhizomes (*Curcuma longa* L.) in a solar conduction dryer. Inf Process Agric 2015;2(2):85–92.
[35] Balasubramanian S, Sharma R, Gupta RK, Patil RT. Validation of drying models and rehydration characteristics of betel (*Piper betel* L.) leaves. J Food Sci Technol 2011;48(6):685–91.
[36] Kaya A, Aydin O. An experimental study on drying kinetics of some herbal leaves. Energy Convers Manage 2009;50 (1):118–24.
[37] Nuthong P, Achariyaviriya A, Namsanguan K, Achariyaviriya S. Kinetics and modeling of whole longan with combined infrared and hot air. J Food Eng 2011;102(3):233–9.
[38] Doymaz İ. Evaluation of mathematical models for prediction of thin-layer drying of banana slices. Int J Food Prop 2010;13 (3):486–97.
[39] Motevali A, Amiri Chayjan R, Salari K, Taghizadeh A. Studying the effect of different drying bed on drying characteristic of mint leaves. Chem Prod Process Model 2016;11(3):231–9.
[40] Premi M, Sharma HK, Sarkar BC, Singh C. Kinetics of drumstick (*Moringa oleifera*) during convective drying. Afr J Plant Sci 2010;4(10):391–400.
[41] Doymaz İ, Kocayigit F. Drying and rehydration behaviors of convection drying of green peas. Dry Technol 2011;29 (11):1273–82.
[42] Xiao HW, Yao XD, Lin H, Yang WX, Meng JS, Gao ZJ. Effect of SSB (superheated steam blanching) time and drying temperature on hot air impingement drying kinetics and quality attributes of yam slices. J Food Process Eng 2012;35 (3):370–90.